THE PROTEIN SOCIETY

Crystal structure and functional analysis of MiD49, a receptor for the mitochondrial fission protein Drp1

Oliver C. Losón,[1] Shuxia Meng,[1] Huu Ngo,[1] Raymond Liu,[1] Jens T. Kaiser,[2] and David C. Chan[1]*

[1]Division of Biology and Biological Engineering, California Institute of Technology, Pasadena, California 91125
[2]Division of Chemistry and Chemical Engineering, California Institute of Technology, Pasadena, California 91125

Received 24 October 2014; Revised 17 December 2014; Accepted 18 December 2014
DOI: 10.1002/pro.2629
Published online 00 Month 2014 proteinscience.org

Abstract: Mitochondrial fission requires recruitment of dynamin-related protein 1 (Drp1) to the mitochondrial surface, where assembly leads to activation of its GTP-dependent scission function. MiD49 and MiD51 are two receptors on the mitochondrial outer membrane that can recruit Drp1 to facilitate mitochondrial fission. Structural studies indicated that MiD51 has a variant nucleotidyl transferase fold that binds an ADP co-factor essential for activation of Drp1 function. MiD49 shares sequence homology with MiD51 and regulates Drp1 function. However, it is unknown if MiD49 binds an analogous co-factor. Because MiD49 does not readily crystallize, we used structural predictions and biochemical screening to identify a surface entropy reduction mutant that facilitated crystallization. Using molecular replacement, we determined the atomic structure of MiD49 to 2.4 Å. Like MiD51, MiD49 contains a nucleotidyl transferase domain; however, the electron density provides no evidence for a small-molecule ligand. Structural changes in the putative nucleotide-binding pocket make MiD49 incompatible with an extended ligand like ADP, and critical nucleotide-binding residues found in MiD51 are not conserved. MiD49 contains a surface loop that physically interacts with Drp1 and is necessary for Drp1 recruitment to the mitochondrial surface. Our results suggest a structural basis for the differential regulation of MiD51- versus MiD49-mediated fission.

Keywords: mitochondrial fission; mitochondrial dynamics; MiD49; dynamin-related protein

Broad audience statement

Mitochondria are dynamic organelles that continually fuse and divide. Mitochondrial division requires recruitment of dynamin-related protein 1 (Drp1) to the surface of mitochondria. MiD49 and MiD51 are two mitochondrial proteins that recruit Drp1 to the mitochondrial surface. We have solved the structure of MiD49 and found that it has structural differences from MiD51 that may explain their differential regulation of mitochondrial division.

Additional Supporting Information may be found in the online version of this article.

*Correspondence to: David C. Chan; California Institute of Technology, 1200 E. California Boulevard, MC114-96, Pasadena, CA 91125. E-mail: dchan@caltech.edu

Introduction

Fusion and division (fission) regulate mitochondrial shape and function, and the balance of these opposing processes is tightly controlled.[1–3] Disruption of either process causes disease in humans and mid-gestational lethality in mouse models.[4–10]

In mammals, mitochondrial fission requires the recruitment of a large GTPase called dynamin related protein 1 (Drp1) to the mitochondrial surface. Analogous to classical dynamin on the neck of endocytic vesicles, Drp1 (or Dnm1 in yeast) oligomerizes around the circumference of the mitochondrion, and its GTP hydrolysis activity is thought to power membrane constriction and scission.[11,12] Recombinant Drp1 can form ordered oligomers *in vitro* and deform liposomes.[12–14] This oligomerization promotes its GTP hydrolysis activity,[11] which is essential for mitochondrial fission.

Published by Wiley-Blackwell. © 2014 The Protein Society

Four integral outer membrane proteins independently recruit Drp1 to mitochondria: Fission 1 (Fis1), Mitochondrial Fission Factor (Mff), and Mitochondrial Dynamics proteins of 49 and 51 kDa (MiD49 and MiD51). Early studies suggested that Fis1 is important for fission,[15–18] but more recent studies with knockout cells indicate that Fis1 has little or no role in mitochondrial fission.[19,20] In contrast, Mff is critical for the recruitment of Drp1 and regulation of mitochondrial morphology in several cell types.[19–21]

MiD49 and MiD51 also regulate Drp1 recruitment, but they appear to induce mitochondrial fission only under certain cellular contexts. When overexpressed, these proteins cause robust recruitment of Drp1 to mitochondria, but fission activity is inhibited, resulting in dramatic elongation of mitochondria.[22–25] Treatment of MiD51-overexpressing cells with carbonyl cyanide *m*-chlorophenylhydrazone (CCCP), which causes loss of mitochondrial membrane potential, promotes rapid mitochondrial fission.[20] Drp1 recruited by MiD49 overexpression can also be activated for fission by this treatment, but to a lesser degree. In addition, treatment with the respiration inhibitor antimycin A robustly activates fission in MiD51-overexpressing cells but not in MiD49-overexpressing cells.[14] It is unknown how MiD49 and MiD51 respond differentially to distinct cellular signals. Structural studies demonstrated that MiD51 contains a variant nucleotidyl transferase (NTase) domain that is probably enzymatically inactive. Instead, it stably binds to ADP as a cofactor (and GDP with lower affinity).[14,26]

In order to better understand the functional differences between MiD49 and MiD51, we determined the atomic structure for the cytosolic domain of recombinant mouse MiD49. Because native MiD49 was refractory to crystallization, we created a library of surface entropy reduction (SER) mutants based on a predicted structure derived from the atomic model of MiD51. One of these mutants, R218A, facilitated crystallization and structure determination. Like MiD51, MiD49 contains a nucleotidyl transferase (NTase) domain. However, the domain in MiD49 has a modified binding pocket that is incompatible with ADP binding. In addition, the MiD49 structure lacks key residues involved in nucleotide binding and is not a dimer. The structural differences between MiD49 and MiD51 may provide an explanation for their differential regulation of Drp1-mediated fission.

Results

Crystallization of the cytosolic segment of MiD49

Extensive attempts to crystallize the cytosolic region of MiD49 failed to identify promising hits. Following the strategy that led to crystallization of MiD51,[14] we performed limited proteolysis on recombinant MiD49 to identify a stable core. N-terminal peptide sequencing combined with mass spectrometry revealed that proteolysis removed the N-terminal region (up to position 124), which was predicted to lack secondary structure. Based on these proteolysis results, we generated new constructs to produce the protease-resistant core (MiD49Δ1–124, Δ1–125, and Δ1–126). These new constructs expressed and purified well but still failed to crystallize.

Surface entropy reduction (SER) is an approach to facilitate the crystallization of proteins. Surface residues with side groups that have high flexibility and polarity can impede crystallization because they inhibit necessary intermolecular interactions.[27] To identify such surface residues on MiD49, we created a predicted structure of MiD49Δ1–124 through the I-TASSER server,[28] with structural restraints from the MiD51 model as a template [Fig. 1(A)]. The cytosolic segments of MiD49 and MiD51 share 42% sequence similarity, and as expected, the predicted structure of MiD49 is very similar to that of MiD51. We inspected the surface of the predicted MiD49 structure for residues having side chains believed to cause high entropy, including arginine, lysine, glutamine, and glutamate.[29,30] After initial inspection, the suspect residues and neighboring sequences were compared against that of homologous segments in MiD51. Residues and surrounding sequences showing little chemical conservation were considered prime targets for mutagenesis. Polar residues with no neighboring moiety to coordinate their charge were also targeted. Additionally, we included residues with large side-chains conspicuously protruding from the surface. Selected residues were grouped into clusters, and 12 MiD49Δ1–125 mutants containing 1–3 alanine substitutions were made (Fig. 1).

The 12 SER mutants were screened for solubility in small-scale cultures [Fig. 1(B)]. Mutants showing solubility comparable to or better than wildtype MiD49 were grown in large scale for purification and crystal trials. Of the 12 SER mutants, only the R218A single point mutant produced crystals, as evaluated by sparse matrix crystallization screens. We also combined the R218A mutation with four other SER mutation clusters, but the compound mutations did not substantially improve crystallization.

Structural differences between the nucleotidyl transferase domains of MiD49 and MiD51

R218A mutant crystals diffracted to high resolution and we solved the structure by molecular replacement with a poly-serine substituted version of our MiD51 model (Supporting Information Table S1). The structure was solved at a resolution of 2.4 Å (Supporting Information Table S1). Model building and refinement produced a final structure with

A

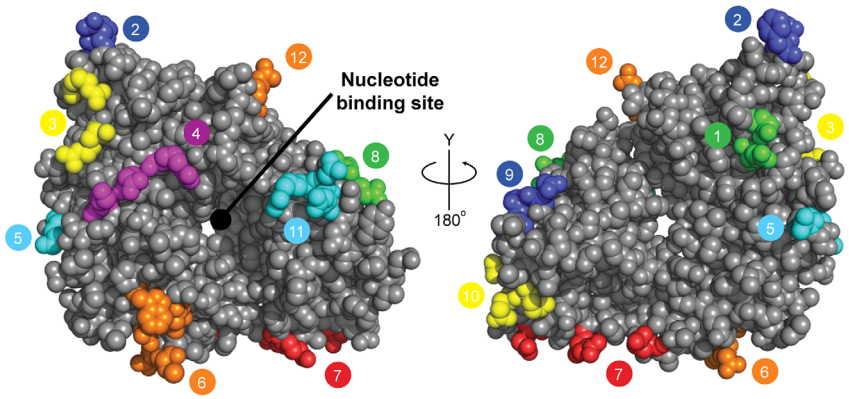

B

SER CLUSTER	MUTANT RESIDUES	SOLUBILITY	CRYSTAL
WT	–	****	No
1	E201A, E203A	*	–
2	E231A, F232A	******	No
3	R235A, R242A	****	No
4	R252A, E256A, K260A	*	–
5	R165A, K167A	******	No
6	E295A, C296A, E298A	***	–
7	E129A, R136A, K137A	*	–
8	E406A, E413A, Q414A	***	No
9	E387A, E388A, E389A	****	No
10	E394A, E395A, E399A	*	–
11	R432A, E433A, E434A	***	No
12	R218A	***	Yes
11+12	R218A, R432A, E433A, E434A	***	Yes
3+12	R218, R235A, R242A	***	Yes
5+12	R218A, R165A, K167A	******	Yes
8+12	R218A, E406A, E413A, Q414A	**	–

Figure 1. Crystallization of MiD49 by screening of surface entropy reduction mutants. (A) Sphere representation of the mouse MiD49Δ1–124 structure predicted by the I-TASSER server, with each surface entropy reduction (SER) cluster highlighted in a different color. Residues were selected as SER candidates by inspecting the protein surface and choosing prominent and/or charged residues. SER clusters were generated by grouping neighboring candidate residues. (B) List of SER clusters and the corresponding mutations. In addition to 12 original clusters, an additional four compound clusters were studied. Each is colored as in (A). The behavior of the mutants in solubility and crystallization screens is indicated. WT, wildtype.

excellent stereochemistry, with R_{free} of 24.4% and R_{work} of 20.9%. Like wildtype MiD49, the R218A mutant is capable of recruiting endogenous Drp1 to mitochondria [Fig. 4(D)].

MiD49Δ1–125 has an NTase fold that consists of a central β-strand region flanked by two α-helical regions [Fig. 2(A,B)]. NTase proteins typically catalyze the polymerization of nucleic acids from triphosphate nucleotides. They bind nucleotide triphosphates in the cleft located between the central β-sheet and the C-terminal α-helical segment.[31] When we solved the earlier structure for MiD51, we found that the nucleotide-binding pocket contained additional electron density due to tightly bound ADP.[14] Structural alignments between MiD51 and NTase enzymes showed that residues canonically used for nucleotide binding are only partially conserved in MiD51, resulting in the change from nucleotide triphosphate (found in canonical NTases) to nucleotide diphosphate (ADP) binding. MiD51 uses a triad of residues from the β-sheet segment (H201, Q203, and D311) and two other residues from α-helix 3 (S189) and α-helix 9 (K368) to bind ADP.

Notably, the electron density of MiD49 does not contain any additional peaks in the putative nucleotide-binding pocket [Fig. 3(A,B)]. In addition, with the exception of the histidine (H193 in MiD49), the nucleotide binding residues described above for MiD51 are not conserved in MiD49 [Supporting Information Fig. S1(A)]. The degree of divergence in key residues lining the pocket suggests that MiD49 does not bind any nucleotide-related species. In fact, ligand-binding assays, which identified ADP and GDP as co-factors for MiD51,[14] have failed to yield any candidates for MiD49.

This figure also includes an iMolecules 3D interactive version that can be accessed via the link at the bottom of this figure's caption.

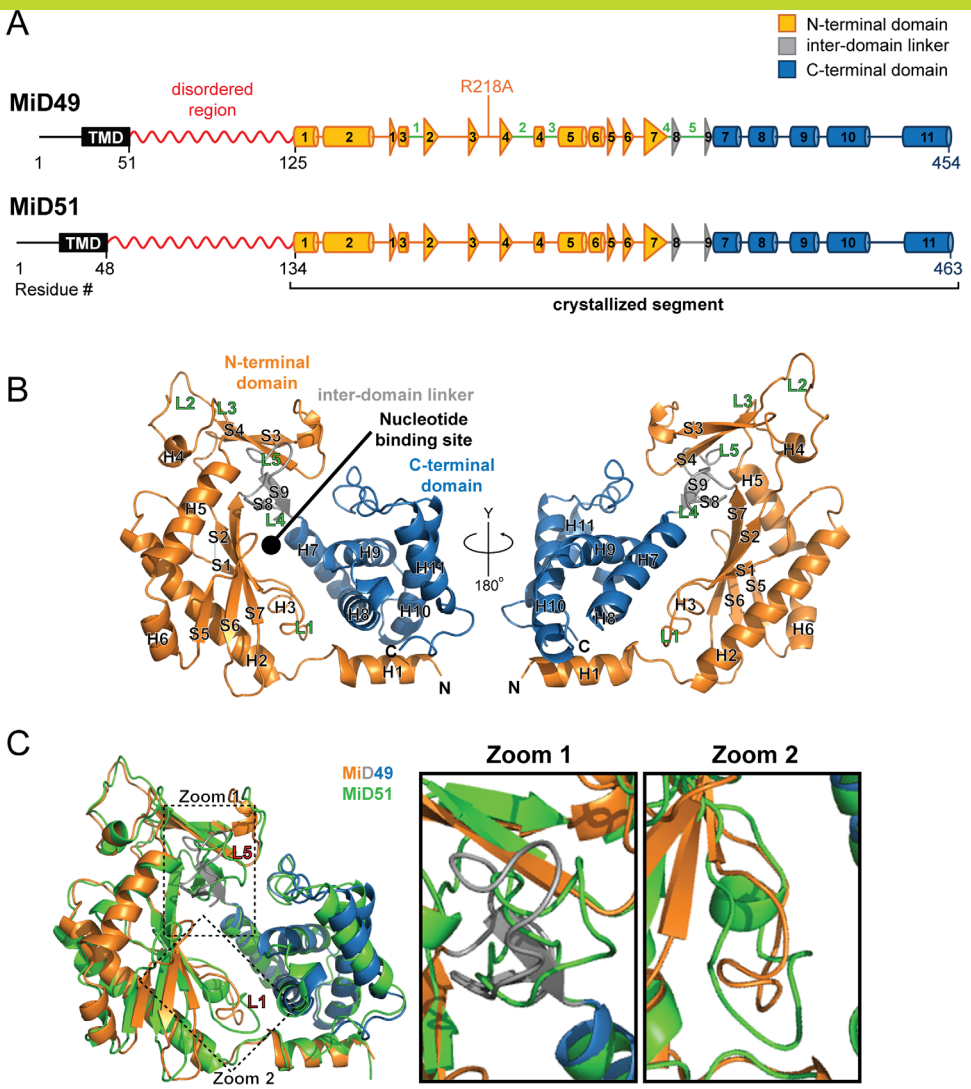

Figure 2. Overview of the MiD49 structure. (A) Schematic of MiD49 and MiD51. The region determined by X-ray crystallography is indicated and color-coded as in (B). The red squiggle indicates a region predicted to lack secondary structure. TMD, transmembrane domain. Cylinders represent α-helices, and triangles represent β-strands. Loops of structural and/or functional relevance are numbered in green. R218A, the SER mutation allowing crystallization. (B) Ribbon representation of mouse MiD49Δ1–125. Orange, N-terminal domain; gray, interdomain linker; blue, C-terminal domain. α-helices and β-strands are numbered according to (A). N and C denote the N and C termini. The black circle indicates the putative nucleotide-binding pocket. (C) Structural overlay of MiD49 (colored as in B) and MiD51 (green). As described in the main text, the L1 and L5 loops (labeled) that line the binding pocket show significant structural differences. These two regions are magnified in the two zoom images on the right. An interactive view is available in the electronic version of the article

The NTase domains of MiD49 and MiD51 show important structural differences in the nucleotide-binding pocket [Fig. 2(C), Supporting Information Fig. S1(A)]. β-strands 5, 6, 7, and 2 that form the central β-sheet region are shifted inwardly in MiD49. Loop 1 (between α-helix 3 and β-strand 2) partially obstructs the opening of the binding cleft, whereas in MiD51 it points away from the opening. Additionally, loop 5 (between β-strands 8 and 9), which lines the top of the binding cleft, is cocked towards the N-terminal α-helical bundle in MiD49. Together, these differences cause the binding pocket in MiD49 to be shallower and to have a narrowed opening [Supporting Information Fig. S1(B)]. When the ADP co-factor from MiD51 is superimposed onto the MiD49 structure, it is clear that the smaller pocket in MiD49 cannot accommodate the nucleotide (Fig. 3). Residues 192E (from Loop 1) and 375W (from helix 9) clash with the terminal β-phosphate group. At the opposite end of ADP, the adenine ring clashes with residue 195R (from β-strand 2) and 333D (from β-strand 9) [Fig. 3(C)]. These structural changes in the pocket, along with divergence of the nucleotide binding residues, likely

explain the apparent inability of MiD49 to bind nucleotides.

In addition to the structural differences in and around the binding cleft, the loop segment found between β-strands 7 and 8 (loop 4) differs between MiD49 and MiD51. This loop segment is found on the surface that is behind the cleft, and shows a substantial downward shift towards the membrane proximal surface in MiD49 as compared to MiD51 [Supporting Information Fig. S2(A)]. This movement causes the loop to protrude from the surface of MiD49 more saliently. Interestingly, an MiD51 mutant incapable of forming a homodimer has a similar downward shift in this loop [Supporting Information Fig. S2(A)]. This mutant can interact with and recruit Drp1 but cannot activate fission.[14] In our crystal structure, MiD49 does not form a dimer, and the residues used by MiD51 to mediate dimerization are not conserved in MiD49 [Supporting Information Fig. S2(B)].

Identifying the Drp1-binding motif on MiD49

We previously identified an MiD51 surface segment—encompassing loop 2, α-helix 4, and loop 3—which binds to Drp1.[14] MiD49 and MiD51 have high sequence homology in this region [Fig. 4(A)], and the two structures superimpose well [Fig. 4(B)]. A key structural component of this region in MiD49 is a salt bridge between Arg227 from loop 2 and Asp241 from α-helix 4. We and others found that the analogous salt bridge in MiD51 (between Arg235 and Asp249) is critical to the stability of the loop structure and for recruitment of Drp1.[14,26]

To test whether this region is important for binding Drp1, we analyzed mutants designed to disrupt this surface segment. These mutants were expressed in human cells and tested for Drp1-binding in a co-immunoprecipitation assay [Fig. 4(C)]. In loop 2, mutation of Arg227 to alanine, which ablates the salt bridge, caused a dramatic decrease in Drp1 interaction. Other loop 2 (L230G) or α-helix 4 (R242A) point mutations had little effect on Drp1 binding, but a compound (229QLEFHPR235 → 229AGVGAPA235) loop 2 mutant had a moderate reduction. In loop 3, the V245E/G246E mutation caused a dramatic loss of MiD49-Drp1 binding similar to R227A. The homologous regions in MiD51 were determined to also be important for MiD51-Drp1 binding.[14]

We next tested the ability of these mutants to recruit Drp1 to mitochondria [Fig. 4(D)]. Exogenous expression of either MiD49 or MiD51 can rescue recruitment of Drp1 foci to mitochondria of *Fis1*/*Mff*-null cells. These mutant cells normally show little recruitment of Drp1 to mitochondria, with most of the Drp1 appearing cytosolic.[20] Mirroring the defect seen in the co-immunoprecipitation assay, both the R227A and the V245E/G246E mutants showed a strong defect in recruiting Drp1. The compound loop 2 mutant showed a less severe but clear defect.

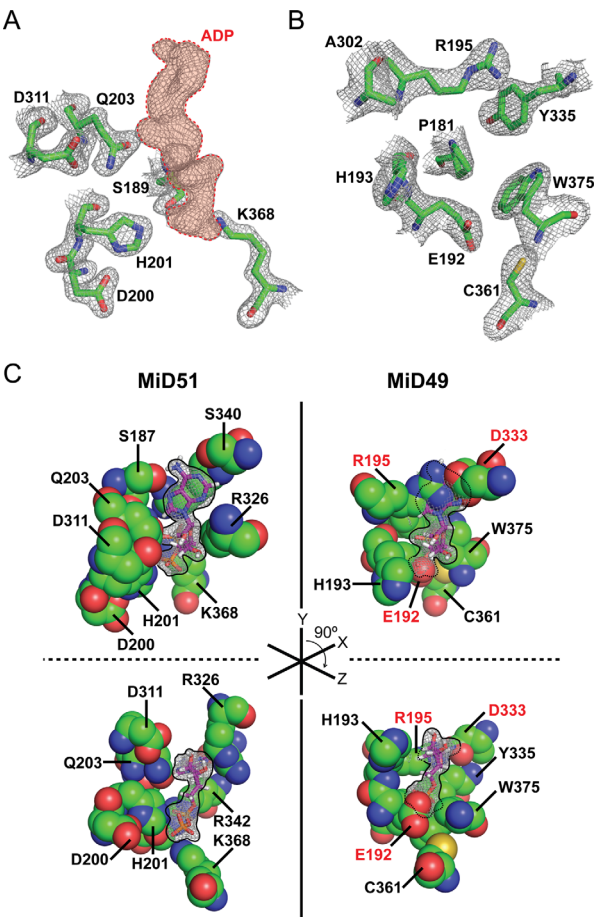

Figure 3. Lack of ligand density in MiD49 map. (A) The electron 2mFo-DFc density of native MiD51 contains extra peaks (outlined in red) in the binding cleft. This density corresponds to ADP and is present even though the protein was extensively purified in the absence of nucleotide. (B) No extra density is found in the binding cleft of MiD49. In (A) and (B), NTase nucleotide binding residues are depicted as sticks. For MiD49, Y325 and W375 are additionally depicted because of their significant occupation of the binding cleft. (C) The 2mFo-DFc for ADP (gray mesh outlined in black) is depicted in the binding cleft of MiD51 (left) and superimposed on MiD49 (right). Residues from (A) and (B) are depicted as spheres, and ADP is depicted in stick representation. The black outline is dashed where the ADP electron density clashes with residues. In MiD49, the three residues (E192, R195 and D333) clashing with the ADP density are labeled in red. The two mFo-FDc maps in (A), (B), and (C) are contoured at 1.2σ.

Discussion

By comparing the structures of MiD49 and MiD51,[14,26] we have uncovered structural similarities and differences between these two Drp1 receptors. Both proteins contain noncanonical NTase domains that have a modified binding pocket and do not appear to retain an enzymatic function. MiD51 binds nucleotide diphosphates (ADP and GDP),

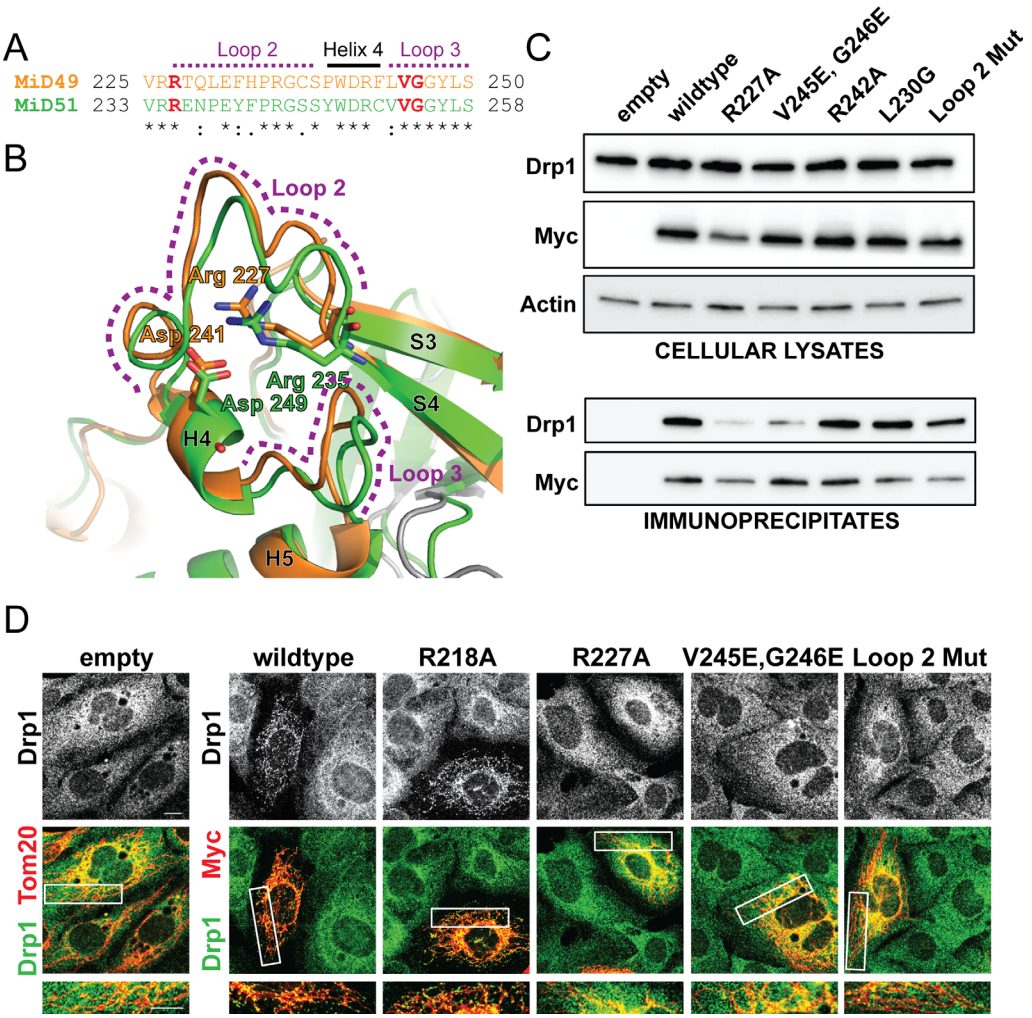

Figure 4. Drp1-binding motif on MiD49. (A) Sequence alignment of the Drp1 binding region. Red, residues found to be critical for Drp1 binding by MiD49 (this study) and MiD51 (14). Orange, MiD49; Green, MiD51. Sequence similarity symbols: asterisk, fully conserved; colon, highly conserved; period, weakly conserved. (B) Structural overlay of MiD49 (colored as in Fig. 2B) and MiD51 (green). α-helices and β-strands are numbered according to Figure 2A. The dotted purple lines highlight loops 2 and 3, which house residues important for Drp1 binding. Both MiD49 and MiD51 contain an Arg-Asp pair that forms a salt bridge critical to local structural integrity. (C) Analysis of MiD49-Drp1 binding in 293T cells. Wildtype or mutant MiD49-Myc was co-expressed with mouse Drp1, and Myc-immunoprecipitates were analyzed for Drp1. Top, expression of Drp1, MiD49-Myc, and actin (loading control) in cell lysates. Bottom, anti-Myc immunoprecipitates analyzed for Drp1. The loop 2 Mut sequence is 229 AGVGAPA 235. (D) Analysis of mitochondrial Drp1 recruitment in *Fis1/Mff*-null cells expressing MiD49-Myc variants. *Fis1/Mff*-null cells have extremely low levels of Drp1 on mitochondria.[20] Consistent with this finding, control cells expressing empty vector (far left) have diffuse anti-Drp1 staining (green), with most of the staining residing outside the mitochondria (inset at bottom). Mitochondria were visualized by anti-Tom20 (red). In cells expressing MiD49-Myc or variants (right five panels), transfected cells were identified by anti-Myc staining (red), which also highlights the mitochondria. Expression of wildtype MiD49 results in punctate localization of Drp1 to mitochondria, leaving little in the cytosol (second column, bottom panel). In contrast, the R227A and V245E/G246E mutants show diffuse Drp1 staining with poor localization to mitochondria. Consistent with the immunoprecipitation results, the Loop2 mutant shows only a subtle defect. The R218A SER mutation does not affect Drp1 recruitment by MiD49. Scale bars, 10 μm. Regions within the white boxes are shown in greater magnification below.

rather than nucleotide triphosphates, as co-factors critical for function.[14,26]

In contrast, MiD49 shows more extreme structural and sequence variations in the nucleotide-binding pocket. The changes in the pocket are caused by repositioning of the central β-sheet region and the loops flanking the binding pocket. These changes reduce the size and depth of the pocket, making it incompatible with an extended ligand like ADP. Consistent with the lack of ligand in the crystal structure, our attempts to identify a co-factor have been negative. Nevertheless, it remains possible that MiD49 binds a yet unknown ligand with a faster off rate than that of ADP for MiD51. The extensive divergence in the nucleotide binding residues, however, suggests that if a ligand does exist, it will be of a different class.

Another difference between the MiD49 and MiD51 crystal structures is that MiD49 adopts a

monomer structure, whereas MiD51 is dimeric. The dimeric structure of MiD51 would seem to be well suited to recruit the basal state of Drp1, which is believed to be dimeric. It is possible that MiD49 has weak dimerization that is not detectable in the truncated form of MiD49 (lacking the transmembrane segment) used for crystallization. Alternatively, if MiD49 is indeed a monomer, it may facilitate a different arrangement of Drp1 that may have an impact on its fission activity.

The differences in ligand binding between MiD51 and MiD49 may underlie their differential regulation of mitochondrial fission. Although mitochondrial fission can be activated by CCCP in cells overexpressing MiD51 or MiD49, the response is substantially stronger in MiD51 expressing cells. Antimycin A, which inhibits complex III of the electron transport chain, selectively activates mitochondrial fission in cells overexpressing MiD51 but not cells overexpressing MiD49. We speculate that ADP binding by MiD51 may enable it, but not MiD49, to be responsive to metabolic changes in the cell.

Materials and methods

Materials

Antibody sources: Drp1 (BD Biosciences), Tom20 (Santa Cruz), Actin (Millipore), Myc (mouse monoclonal 9E10, Covance; rabbit polyclonal, Sigma-Aldrich). Cells were grown in LabTek chambered glass slides (Nunc) for fixed cell imaging. Dithiobis(-succinimidyl propionate) (DSP) was purchased from Thermo-Pierce. Crystallization screens were from Hampton Research and Emerald Biosciences.

Protein structure prediction

The I-TASSER server builds 3D models of proteins based on multiple-threading alignments using the local meta-threading-server (LOMETS) and iterative template fragment assembly simulations (http://zhanglab.ccmb.med.umich.edu/I-TASSER/). Chain A from Protein Data Bank model 4OAF (native MiD51Δ1–133) was used as a template to guide I-TASSER modeling of MiD49Δ1–124. Similar results were obtained using the structures of cyclic GMP-AMP synthase or human MiD51 as templates.

Recombinant protein production and purification

The relevant portion of the mouse MiD49 coding sequence (NCBI Reference Sequence: NP_001009927.1) was amplified from mouse embryonic day 10.5 total RNA. Recombinant proteins were produced in Rosetta (DE3) BL21 *E. coli* (Invitrogen). One liter of terrific broth (TB) containing 100 μg/mL ampicillin and 50 μg/mL chloramphenicol was grown at 37°C to an OD_{600} of 1.5. Cultures were cooled on ice for 30 min and induced with 1 m*M* isopropyl β-D-1-thiogalactopyranoside (IPTG) overnight at 16°C. The cells were harvested and stored at −80°C. Pilot cultures were grown in 50 mL TB to an OD_{600} of 1.5. For a typical purification, 10 g of cells expressing MiD49 protein were lysed in 50 mL GST buffer (50 m*M* HEPES, 300 m*M* NaCl, 10% glycerol, 2 m*M* DTT, pH 7.4) with sonication. Lysates were cleared by centrifugation at 43,000 *g* for 30 min at 4°C. GST tagged MiD49 proteins were captured with glutathione sepharose (GE Healthcare) and washed with GST buffer. The beads were then exchanged into protease buffer (50 m*M* HEPES, 150 m*M* NaCl, 2 m*M* DTT, pH 7.4). PreScission Protease (80 units, GE Healthcare) was incubated for 20 hours at 4°C with continuous end-over-end mixing. The eluted protein was further purified by size exclusion on a Hi-Load Superdex 200 16/60 column (GE Healthcare) pre-equilibrated with GST column buffer (20 m*M* HEPES, 150 m*M* NaCl, 2 m*M* DTT, pH 7.4) and driven by an AKTA Purifier (Amersham). Peak fractions were collected and concentrated to approximately 2 m*M* using Amicon Ultra-15 concentrators (Millipore) with a molecular weight cutoff of 10 kDa. Proteins were flash-frozen in liquid nitrogen and stored at −80°C.

Limited proteolysis of MiD49Δ1–51 was performed with 1 μg/μL recombinant protein and 0.001 μg/μL trypsin (Promega) at 4°C. Time points were taken by diluting aliquots in Laemmli buffer (25 m*M* Tris, 10% glycerol, 1% SDS, 0.01% Bromophenol Blue, 2% β-mercaptoethanol, pH 6.8) and boiling samples immediately.

Crystallization, data collection, and structure determination

Crystallization trials were performed using the hanging drop-vapor diffusion method at room temperature, and identified a condition [100 m*M* HEPES (pH 7.0), 20 m*M* $MgCl_2$, 20% polyacrylic acid 5,100 (w/v),] that yielded rod-shaped crystals for R218A. No crystallization condition was found for wildtype. Diffraction data were collected from vitrified crystals on beamline 12-2 at the Stanford Synchrotron Radiation Lightsource. All data were processed with XDS,[32] and merged using SCALA[33] as implemented in CCP4.[34]

Molecular replacement was performed using a single molecule from the mouse MiD51 structure (PDB ID 4OAF) using PHASER[35] in PHENIX[36] with a 2.2 Å data set. Replacement with this structure did not yield an interpretable density. Use of a polyserine-substituted version of MiD51 resulted in an electron density with many of the side chain densities apparent and secondary structures clearly visible. Refinement was carried out using PHENIX, with an initial round of rigid body refinement followed by a round of simulated annealing. After a few rounds of refinement with TLS obtained from

the TLSMD server,[37] the R_{work} converged to 20.9% and the R_{free} to 24.4%. No density was present in the binding cleft after refinement was finalized. The final model includes residues 126–454 and has excellent stereochemistry with few Ramachandran outliers, as assessed by MOLPROBITY.[38]

The structure has been deposited at the Protein Data Bank under PDB ID 4WOY.

Immunofluorescence and imaging

For immunofluorescence, cells were fixed in 4% formaldehyde for 10 min at 37°C, permeabilized with 0.1% Triton-X100 at room temperature, and incubated with antibodies in 5% fetal calf serum in phosphate buffered saline. Bound antibody was visualized with Alex Fluor conjugated secondary antibodies (Life Technologies).

All fluorescence imaging was performed using a Plan-Apochromat 63X/1.4 oil objective on a Zeiss LSM 710 confocal microscope driven by Zen 2009 software (Carl Zeiss). Image cropping and global adjustments to brightness and contrast were performed using Photoshop (Adobe).

Cell culture

All cell lines were cultured in Dulbeco's modified Eagle's medium (DMEM) containing 10% FBS and supplemented with 100 U/mL penicillin and 100 μg/mL streptomycin.

Cloning and transfection

MiD49 and *Drp1* variant 2 were amplified from a MEF cDNA library using PCR. *MiD49* was cloned into the XhoI and BamHI sites of a pcDNA3.1(-) plasmid containing a C-terminal 4xMyc tag, and *Drp1* was cloned into the BamHI and XhoI sites of pcDNA3.1(+). The entire open reading frames were confirmed by DNA sequencing. For recombinant protein expression in bacteria, mouse MiD49Δ1–51 and MiD49Δ1–125 were cloned into the BamHI and XhoI sites of pGEX6P1 (GE Healthcare). All mutants for MiD49 were constructed by PCR using oligonucleotides encoding mutations.

Plasmids were transfected using Lipofectamine 2000 (Invitrogen). Cells transfected with plasmids were assessed 24 hours post-transfection. MiD49-Myc positive cells were visualized with Myc immunofluorescence and mitochondria were visualized with Tom20 immunofluorescence.

Immunoprecipitation

To assess MiD49 interaction with Drp1, mouse MiD49-Myc was co-transfected with mouse Drp1 into 293T cells growing in 35 mm plates. About 24 hours post-transfection, cells were trypsinized, washed once with PBS, and cross-linked with 250 μ*M* DSP in PBS for 20 min at room temperature. Cross-linker was quenched by the addition of Tris pH 7.4 to 100 m*M* final, and cells were washed once with PBS containing 100 m*M* Tris pH 7.4. Cells were lysed in IP buffer (1% Triton X100, 150 m*M* NaCl, 25 m*M* Tris-HCl, 1 m*M* EDTA, pH 7.4) and lysates were cleared with a 21,000 *g* spin at 4°C for 10 min. Immunoprecipitations were performed in IP buffer, and immune complexes were captured with protein A/G agarose (Thermo-Pierce). Beads were washed with IP buffer, and cross-links were reversed by boiling samples in Laemmli buffer containing 5% β-mercaptoethanol.

Acknowledgments

The authors acknowledge the Gordon and Betty Moore Foundation, the Beckman Institute, and the Sanofi-Aventis Bioengineering Research Program at Caltech for their generous support of the Molecular Observatory at Caltech. Operations at SSRL are supported by the US DOE and NIH. This work was supported by the National Institutes of Health (GM110039). OCL was supported by a R. L. Kirschstein National Research Service Award (5F31GM089327) and an American Physiological Society William Townsend Porter Pre-doctoral fellowship.

References

1. Westermann B (2010) Mitochondrial fusion and fission in cell life and death. Nat Rev Mol Cell Biol 11: 872–884.
2. Chan DC (2012) Fusion and fission: interlinked processes critical for mitochondrial health. Ann Rev Genet 46:265–287.
3. Youle RJ, van der Bliek AM (2012) Mitochondrial fission, fusion, and stress. Science 337:1062–1065.
4. Alexander C, Votruba M, Pesch UE, Thiselton DL, Mayer S, Moore A, Rodriguez M, Kellner U, Leo-Kottler B, Auburger G, Bhattacharya SS, Wissinger B (2000) OPA1, encoding a dynamin-related GTPase, is mutated in autosomal dominant optic atrophy linked to chromosome 3q28. Nat Genet 26:211–215.
5. Delettre C, Lenaers G, Griffoin JM, Gigarel N, Lorenzo C, Belenguer P, Pelloquin L, Grosgeorge J, Turc-Carel C, Perret E, Astarie-Dequeker C, Lasquellec L, Arnaud B, Ducommun B, Kaplan J, Hamel CP (2000) Nuclear gene OPA1, encoding a mitochondrial dynamin-related protein, is mutated in dominant optic atrophy. Nat Genet 26:207–210.
6. Chen H, Detmer SA, Ewald AJ, Griffin EE, Fraser SE, Chan DC (2003) Mitofusins Mfn1 and Mfn2 coordinately regulate mitochondrial fusion and are essential for embryonic development. J Cell Biol 160:189–200.
7. Zuchner S, Mersiyanova IV, Muglia M, Bissar-Tadmouri N, Rochelle J, Dadali EL, Zappia M, Nelis E, Patitucci A, Senderek J, Parman Y, Evgrafov O, Jonghe PD, Takahashi Y, Tsuji S, Pericak-Vance MA, Quattrone A, Battaloglu E, Polyakov AV, Timmerman V, Schroder JM, Vance JM (2004) Mutations in the mitochondrial GTPase mitofusin 2 cause Charcot-Marie-Tooth neuropathy type 2A. Nat Genet 36:449–451.
8. Waterham HR, Koster J, van Roermund CW, Mooyer PA, Wanders RJ, Leonard JV (2007) A lethal defect of

mitochondrial and peroxisomal fission. New Engl J Med 356:1736–1741.
9. Ishihara N, Nomura M, Jofuku A, Kato H, Suzuki SO, Masuda K, Otera H, Nakanishi Y, Nonaka I, Goto Y, Taguchi N, Morinaga H, Maeda M, Takayanagi R, Yokota S, Mihara K (2009) Mitochondrial fission factor Drp1 is essential for embryonic development and synapse formation in mice. Nat Cell Biol 11:958–966.
10. Wakabayashi J, Zhang Z, Wakabayashi N, Tamura Y, Fukaya M, Kensler TW, Iijima M, Sesaki H (2009) The dynamin-related GTPase Drp1 is required for embryonic and brain development in mice. J Cell Biol 186: 805–816.
11. Ingerman E, Perkins EM, Marino M, Mears JA, McCaffery JM, Hinshaw JE, Nunnari J (2005) Dnm1 forms spirals that are structurally tailored to fit mitochondria. J Cell Biol 170:1021–1027.
12. Mears JA, Lackner LL, Fang S, Ingerman E, Nunnari J, Hinshaw JE (2011) Conformational changes in Dnm1 support a contractile mechanism for mitochondrial fission. Nat Struct Mol Biol 18:20–26.
13. Koirala S, Guo Q, Kalia R, Bui HT, Eckert DM, Frost A, Shaw JM (2013) Interchangeable adaptors regulate mitochondrial dynamin assembly for membrane scission. Proc Natl Acad Sci USA 110:E1342–1351.
14. Loson OC, Liu R, Rome ME, Meng S, Kaiser JT, Shan SO, Chan DC (2014) The mitochondrial fission receptor MiD51 requires ADP as a cofactor. Structure 22:367–377.
15. Yoon Y, Krueger EW, Oswald BJ, McNiven MA (2003) The mitochondrial protein hFis1 regulates mitochondrial fission in mammalian cells through an interaction with the dynamin-like protein DLP1. Mol Cell Biol 23: 5409–5420.
16. Lee YJ, Jeong SY, Karbowski M, Smith CL, Youle RJ (2004) Roles of the mammalian mitochondrial fission and fusion mediators Fis1, Drp1, and Opa1 in apoptosis. Mol Biol Cell 15:5001–5011.
17. Koch A, Yoon Y, Bonekamp NA, McNiven MA, Schrader M (2005) A role for Fis1 in both mitochondrial and peroxisomal fission in mammalian cells. Mol Biol Cell 16:5077–5086.
18. Yu T, Fox RJ, Burwell LS, Yoon Y (2005) Regulation of mitochondrial fission and apoptosis by the mitochondrial outer membrane protein hFis1. J Cell Sci 118: 4141–4151.
19. Otera H, Wang C, Cleland MM, Setoguchi K, Yokota S, Youle RJ, Mihara K (2010) Mff is an essential factor for mitochondrial recruitment of Drp1 during mitochondrial fission in mammalian cells. J Cell Biol 191: 1141–1158.
20. Loson OC, Song Z, Chen H, Chan DC (2013) Fis1, Mff, MiD49, and MiD51 mediate Drp1 recruitment in mitochondrial fission. Mol Biol Cell 24:659–667.
21. Gandre-Babbe S, van der Bliek AM (2008) The novel tail-anchored membrane protein Mff controls mitochondrial and peroxisomal fission in mammalian cells. Mol Biol Cell 19:2402–2412.
22. Palmer CS, Osellame LD, Laine D, Koutsopoulos OS, Frazier AE, Ryan MT (2011) MiD49 and MiD51, new components of the mitochondrial fission machinery. EMBO Rep 12:565–573.
23. Zhao J, Liu T, Jin S, Wang X, Qu M, Uhlen P, Tomilin N, Shupliakov O, Lendahl U, Nister M (2011) Human MIEF1 recruits Drp1 to mitochondrial outer membranes and promotes mitochondrial fusion rather than fission. EMBO J 30:2762–2778.
24. Liu T, Yu R, Jin SB, Han L, Lendahl U, Zhao J, Nister M (2013) The mitochondrial elongation factors MIEF1 and MIEF2 exert partially distinct functions in mitochondrial dynamics. Exper Cell Res 319:2893–2904.
25. Palmer CS, Elgass KD, Parton RG, Osellame LD, Stojanovski D, Ryan MT (2013) Adaptor proteins MiD49 and MiD51 can act independently of Mff and Fis1 in Drp1 recruitment and are specific for mitochondrial fission. J Biol Chem 288:27584–27593.
26. Richter V, Palmer CS, Osellame LD, Singh AP, Elgass K, Stroud DA, Sesaki H, Kvansakul M, Ryan MT (2014) Structural and functional analysis of MiD51, a dynamin receptor required for mitochondrial fission. J Cell Biol 204:477–486.
27. Derewenda ZS (2004) Rational protein crystallization by mutational surface engineering. Structure 12:529–535.
28. Roy A, Kucukural A, Zhang Y (2010) I-TASSER: a unified platform for automated protein structure and function prediction. Nat Protoc 5:725–738.
29. Baud F, Karlin S (1999) Measures of residue density in protein structures. Proc Natl Acad Sci USA 96:12494–12499.
30. Lo Conte L, Chothia C, Janin J (1999) The atomic structure of protein–protein recognition sites. J Mol Biol 285:2177–2198.
31. Kristiansen H, Gad HH, Eskildsen-Larsen S, Despres P, Hartmann R (2011) The oligoadenylate synthetase family: an ancient protein family with multiple antiviral activities. J Interferon Cytokine Res 31:41–47.
32. Kabsch W (2010) Xds. Acta Crystallogr D 66:125–132.
33. Evans P (2006) Scaling and assessment of data quality. Acta Crystallogr D 62:72–82.
34. Bailey S (1994) The Ccp4 suite—programs for protein crystallography. Acta Crystallogr D 50:760–763.
35. McCoy AJ, Grosse-Kunstleve RW, Adams PD, Winn MD, Storoni LC, Read RJ (2007) Phaser crystallographic software. J Appl Crystallogr 40:658–674.
36. Adams PD, Afonine PV, Bunkoczi G, Chen VB, Davis IW, Echols N, Headd JJ, Hung LW, Kapral GJ, Grosse-Kunstleve RW, McCoy AJ, Moriarty NW, Oeffner R, Read RJ, Richardson DC, Richardson JS, Terwilliger TC, Zwart PH (2010) PHENIX: a comprehensive Python-based system for macromolecular structure solution. Acta Crystallogr D 66:213–221.
37. Painter J, Merritt EA (2006) TLSMD web server for the generation of multi-group TLS models. J Appl Cryst 39:109–111.
38. Davis IW, Leaver-Fay A, Chen VB, Block JN, Kapral GJ, Wang X, Murray LW, Arendall WB, Snoeyink J, Richardson JS, Richardson DC (2007) MolProbity: all-atom contacts and structure validation for proteins and nucleic acids. Nucleic Acids Res 35:W375–W383.